C−H Bond Activation by Sulfated Zirconium Oxide is Mediated by a Sulfur-Centered Lewis Superacid

Jammee, Ratchawi; Kolganov, Alexander; Groves, Marc C.; Pidko, Evgeny A.; Sydora, Orson L.; Conley, Matthew P.

DOI
10.1002/anie.202421699

Publication date
2025

Document Version
Final published version

Published in
Angewandte Chemie - International Edition

How to cite: *Angew. Chem. Int. Ed.* **2025**, *64*, e202421699
doi.org/10.1002/anie.202421699

C–H Bond Activation by Sulfated Zirconia | Hot Paper

C–H Bond Activation by Sulfated Zirconium Oxide is Mediated by a Sulfur-Centered Lewis Superacid

Ratchawi Jammee, Alexander Kolganov, Marc C. Groves, Evgeny A. Pidko, Orson L. Sydora,* and Matthew P. Conley**

Abstract: Sulfated zirconium oxide (**SZO**) catalyzes the hydrogenolysis of isotactic polypropylene (iPP, M_w = 13.3 kDa, $Đ$ = 2.4, $<mmmm>$ = 94 %) or high-density polyethylene (HDPE, M_n = 2.5 kDa, $Đ$ = 3.6) to branched alkane products. We propose that this reactivity is driven by the pyrosulfate sites **SZO**, which open under mild conditions to transiently form adsorbed SO_3 and sulfate groups. This adsorbed SO_3 is a very strong Lewis acid that binds ^{15}N-pyridine or triethylphosphine-oxide (TEPO) ($\Delta E_{ads} > -39$ kcal mol^{-1}), reacts with Ph_3CH to form Ph_3C^+, and mediates H/D exchange in dihydroanthracene-d_4. DFT studies show that pyrosulfate sites open with a modest 26.1 kcal mol^{-1} barrier to form the adsorbed SO_3 and sulfate in the presence of a tetramer of propylene. Hydride abstraction from the tertiary C–H in this model is exothermic and subsequent β-scission forms cleaved products. Analysis of the energetics provided here brackets the hydride ion affinity (HIA) of the adsorbed SO_3 between 226.2 to 237.9 kcal mol^{-1}, among largest values reported for a formally neutral Lewis acid. This study explains how **SZO**, a classic heterogeneous catalyst, can form carbocations by a redox neutral hydride abstraction reaction by very strong Lewis sites.

Introduction

Polymeric hydrocarbon waste is an abundant and inexpensive source of carbon for a future sustainable chemical industry.[1] Chemical modification of polymeric hydrocarbons face similar challenges to those encountered in the chemistry of light alkanes; these contain unpolarized sp^3 hybridized C–H and C–C bonds that are thermodynamically stable and kinetically inert. Reactive catalysts are necessary to activate these unreactive bonds.[2] An example is the mixture of low coordinate zirconium hydrides supported on silica shown in Figure 1a.[3] The Zr–H sites activate a C–H bond in an alkane by a σ-bond metathesis reaction[4] that follows the 4-centered transition state shown in Figure 1b to generate the organozirconium product. A related, yet distinct, heterolytic or 1,2-addition C–H bond activation occurs on oxide surfaces.[5] Figure 1c shows the reaction of an alkane with a ZrO_2 fragment, which follows a similar 4-centered transition state that resembles that for σ-bond metathesis.[6] This reaction is an important chemical step in hydrogenolysis of high density polyethylene catalyzed by amorphous ZrO_2 nanoparticles.[7] The two mechanisms shown in Figure 1b-c are general, and are the dominant reactions that result in the activation of inert C–H bonds on oxide surfaces to form organometallic species.[8] Both mechanisms rely on polarization of a C–H bond by a transition metal that facilitate a formal proton transfer to form the organometallic.

Doping an oxide with H_2SO_4 results in a sulfated oxide. These materials are used in heterogeneous catalysis[9] and as weakly coordinating supports for organometallics.[10] Sulfated zirconium oxide (**SZO**) contains sulfates, pyrosulfates, and Brønsted acid sites.[11] Sulfation would also presumably increase electrophilicity at Zr that is expected to increase rates of heterolytic C–H bond activation reactions.[12] However, there is limited evidence that **SZO** can activate C–H bonds in alkanes by a heterolytic mechanism in Figure 1c, and most proposals assume Brønsted sites on **SZO** protonate C–H bonds to form carbocations. Two notable exceptions to this trend involve reactive pyrosulfate sites. Butane reacts with pyrosulfates on **SZO** to form butenes, H_2O, SO_2 and sulfate.[13] Similar redox reactivity of pyrosulfate sites was also proposed in the chemistry of Cp*IrPh(Me)(PMe_3) with sulfated alumina that forms products through a formal H-atom abstraction from the Cp* ligand.[14]

Pyrosulfate is the acid anhydride formed from sulfate and SO_3, the latter is a very strong Lewis acid. In the proceeding sections we will show that **SZO** contains very strong Lewis sites that we propose are derived from pyrosulfate opening to transient SO_3 and sulfate on the ZrO_2 surface. The Lewis acidic SO_3 interacts strongly with

[*] R. Jammee, M. C. Groves, Prof. Dr. M. P. Conley
Department of chemistry
University of California, Riverside
Riverside, CA, 92521, USA
E-mail: matthew.conley@ucr.edu

Dr. A. Kolganov, Prof. Dr. E. A. Pidko
Inorganic Systems Engineering group
Department of Chemical Engineering
Faculty of Applied Sciences
Delft University of Technology
Van der Maasweg 9, Delft 2629 HZ, The Netherlands
E-mail: E.A.Pidko@tudelft.nl

Dr. O. L. Sydora
Research and Technology
Chevron Phillips Chemical Company LP, Kingwood, Texas, USA
E-mail: sydorol@cpchem.com

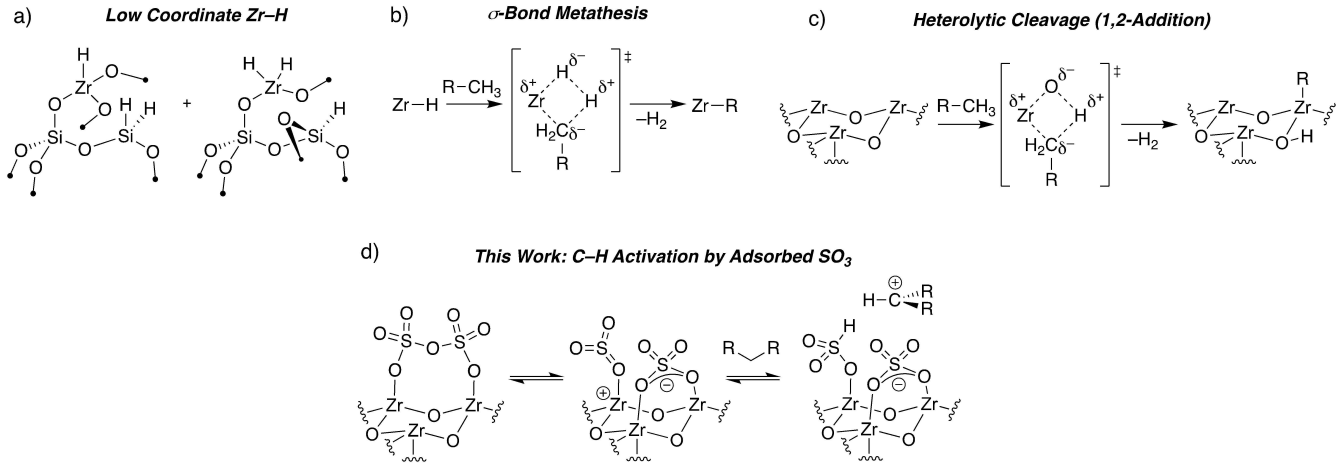

Figure 1. Zr–H supported on partially dehydroxylated silica (a). A σ-bond metathesis reaction of a Zr–H and an alkane (b). A heterolytic cleavage on ZrO_2 (c). Reactivity of adsorbed SO_3 described in this work (d).

common Lewis basic probes and mediates reversible hydride abstraction from hydrocarbons to form carbocations. This reactivity enables **SZO** to mediate chain cleavage in reactions with neat melts of isotactic polypropylene (iPP) or high-density polyethylene (HDPE) in the presence of H_2. These reactions are also initiated by hydride abstraction to form carbocations that undergo β-scission reactions to form cleaved products. Using available heterolytic C–H bond strengths of alkanes that form carbocations on **SZO**, combined with the calculated energies for carbocation formation on a transient SO_3 site, we estimate that the hydride ion affinity between 226.2 to 237.9 kcal mol^{-1}, the largest value reported for a neutral Lewis acid.

Results and Discussion

The **SZO** used for this study was partially dehydroxylated at 300 °C (**SZO_{300}**). **SZO_{300}** contains 2.3 % sulfate (0.72 mmol g^{-1}) from ICP-OES analysis and has 74 m^2 g^{-1} with a moderate loading of Brønsted sites (0.13 ± 0.01 mmol g^{-1}). These loadings translate to ~1.1 Brønsted sites nm^{-2} and ~6 S-containing anions per nm^2. The FTIR of **SZO_{300}** contains a $\nu_{S=O}$ at 1410 cm^{-1}, consistent with pyrosulfate formation (Figure S1).[15] Reactivity of **SZO_{300}** with probes that gauge Lewis acidity are shown in Figure 2. These studies complement previous work using triethylphosphineoxide (TEPO)[16] or ^{15}N-pyridine[17] adsorbed onto **SZO**, and both probes are consistent with the presence of strong Lewis sites on **SZO_{300}**.

The ^{15}N{^{1}H} cross polarization magic angle spinning (CPMAS) NMR spectrum of **SZO_{300}** contacted with ^{15}N-pyridine after evacuation at room temperature for 30 min contains a signal at 200 ppm assigned to pyridinium sites and a second signal at 271 ppm for pyridine adducts of SO_3 (see the Supporting Information). At higher pyridine surface coverage a third signal at 277 ppm appears, which is assigned to either weak Brønsted or weak Lewis sites (Figure S12).[17] The FTIR of this material contains three new $\nu_{S=O}$ bands at 1405, 1377, 1347 cm^{-1}; indicating that the pyrosulfate reacts with pyridine.

The ^{31}P{^{1}H} MAS NMR of **SZO_{300}** after triethylphosphineoxide (TEPO) adsorption at 100 °C contains a signal at 71 ppm and a broad signal centered at ~77 ppm that is typical of Brønsted sites interacting with TEPO.[18] This spectrum also contains a sharp signal at 96 ppm assigned to the TEPO*SO_3 adduct (Figure S6). To place this value in context, similar ^{31}P NMR chemical shifts are usually observed for TEPO adducts of silylium-like ions,[19] which are exceptionally strong Lewis acids.[20] This trend holds with silylium-like ions on surfaces, TEPO contacted [^{i}Pr$_3$Si]-[**SZO**] has a ^{31}P NMR chemical shift of 93 ppm.[21] Similar to pyridine adsorption experiments, the FTIR spectrum of **SZO_{300}** after TEPO adsorption contains a $\nu_{S=O}$ band at 1334 cm^{-1}, showing that pyrosulfate reacts with TEPO.

To rationalize these experimental observations, and to build support for the formation of these SO_3 adducts, periodic DFT calculations at the PBE–D3BJ level were carried out on tetragonal ZrO_2 surface models modified by sulfate and pyrosulfate species. This model also contains Brønsted sites that have similar structures to those reported previously.[22] An excerpt of this model is shown in Figure 2a. This model contains a pyrosulfate flanked by three sulfate anions to approach the experimental values obtained from ICP-OES data. Adduct formation between TEPO or pyridine to the pyrosulfate site results in formation of the TEPO*SO_3 ($\Delta E_{ads} = -50.2$ kcal mol^{-1}) or pyridine*SO_3 ($\Delta E_{ads} = -39.7$ kcal mol^{-1}) adducts, respectively. These adduct formation energies are more exothermic than those calculated from adsorption of TEPO or pyridine onto bare Zr-Lewis sites on a model containing fewer sulfate ions to allow binding to accessible Zr (ΔE_{ads}(py) = −32.3 kcal mol^{-1}; ΔE_{ads}(TEPO) = −45.4 kcal mol^{-1}). The calculated ^{31}P NMR chemical shift of TEPO*SO_3 is 96 ppm, in excellent agreement with experimental values (Table S4).

The calculated structures of TEPO*SO_3 and pyridine*-SO_3 have tetrahedral structures, as expected. The N–S bond length is 1.839 Å and the sum of the O–S–O bond angles

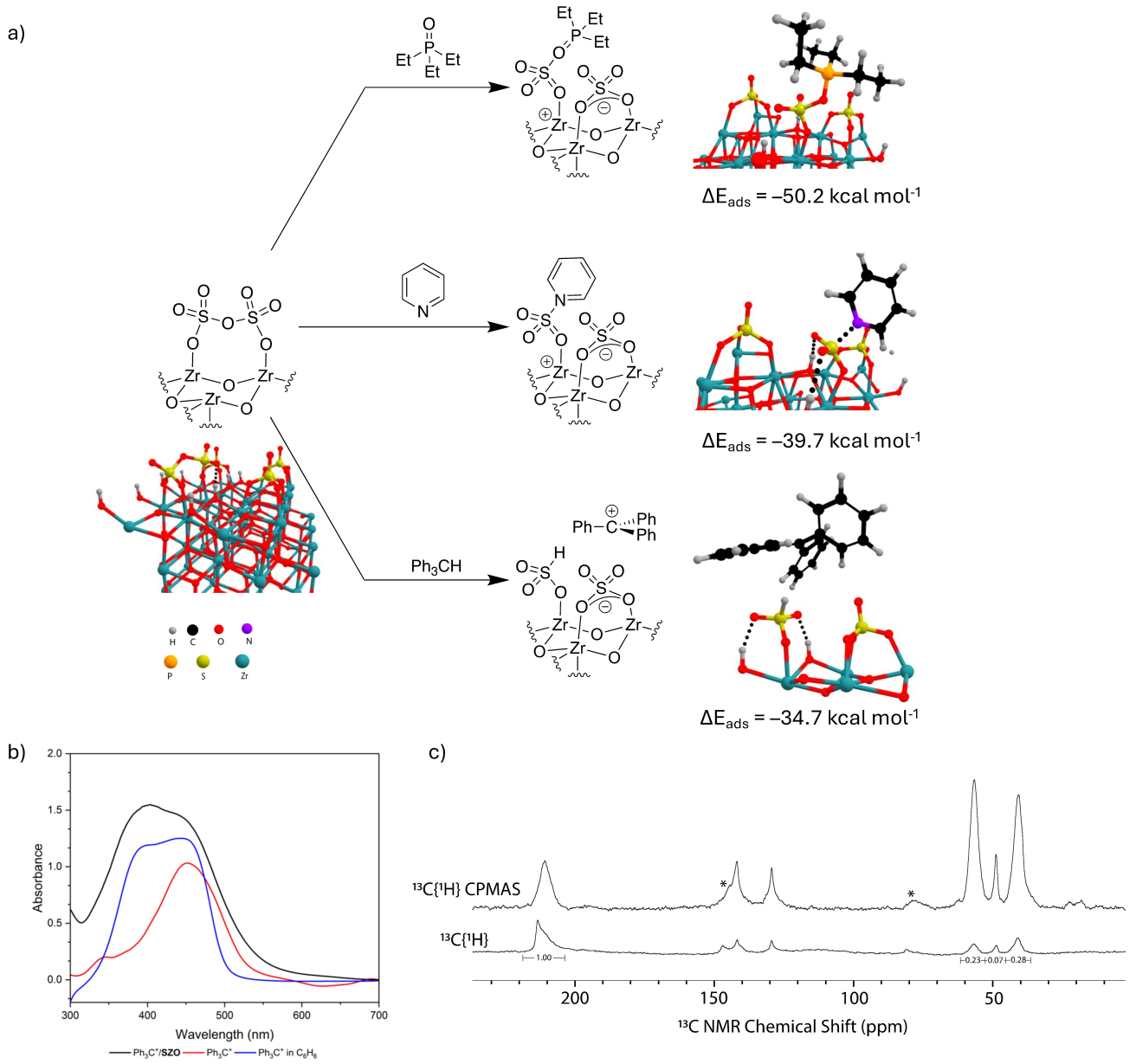

Figure 2. Reaction Scheme for **SZO$_{300}$** (a). The DFT models of **SZO$_{300}$**, TEPO*SO$_3$, pyridine*SO$_3$, and [Ph$_3$C][**SZO$_{300}$**] are shown next to the each structure and calculated energies are given below the calculated structures. DRUV/Vis of [Ph$_3$C][**SZO$_{300}$**][(black), solution UV/Vis of [Ph$_3$C][B(C$_6$F$_5$)$_4$] in C$_6$H$_6$ (blue), DRUV/Vis of [Ph$_3$C][B(C$_6$F$_5$)$_4$] (red, b). ^{13}C{^{1}H} CPMAS NMR spectrum of [Ph$_3$C][**SZO$_{300}$**][(top spectrum), and ^{13}C{^{1}H} MAS NMR spectrum of [Ph$_3$C][**SZO$_{300}$**][(bottom spectrum, c). The numbers under the peaks in the bottom spectrum are integrals for each respective signal. For both experiments ν_{rot} = 10 kHz. Spinning side bands marked with a "*". The bottom spectrum was acquired with a 15 s delay between scans.

(Σ_{OSO}) is 348.3. The S–O bond lengths are 1.441, 1.442, and 1.474, respectively. The longest S–O bond is also interacting with a zirconium on the surface. These metrics are very similar to crystallographically characterized pyridine*SO$_3$[23] (Σ_{OSO} = 348.2; d_{N-S} = 1.828(5) Å, $d_{S=O}$ = 1.416(5), 1.421(6), and 1.429(5) Å, respectively). These bond length and angle patterns are also observed in the TEPO*SO$_3$ adduct, but pyramidalization is more significant (Σ_{OSO} = 332.85), which is reflective of the stronger adduct formed between TEPO and the pyrosulfate compared to pyridine.

Triphenylmethane (Ph$_3$CH) reacts with **SZO$_{300}$** to form [Ph$_3$C][**SZO$_{300}$**], Figure 2a. Monitoring this reaction by ^{1}H NMR spectroscopy shows small amounts of benzene and diphenylmethane also form (Figure S17). Signals for Ph$_3$C$^+$, which would be evidence for leaching from the support, were not detected in these experiments. The diffuse reflectance UV/Vis (DRUV) spectrum of [Ph$_3$C][**SZO$_{300}$**] shown in Figure 3b contains a broad band with λ_{max} at 403 and 436 nm, respectively. These bands are also observed for [Ph$_3$C][B(C$_6$F$_5$)$_4$] in C$_6$H$_6$ solution, and the λ_{max} at 445 is observed by DRUV in solid [Ph$_3$C][B(C$_6$F$_5$)$_4$]. The FTIR of [Ph$_3$C][**SZO$_{300}$**] contains $\nu_{S=O}$ bands at 1393, 1372, and 1359 cm^{-1}, consistent with pyrosulfate reacting with Ph$_3$CH.

Reacting **SZO$_{300}$** with $Ph_3{}^{13}CH$ forms $[Ph_3{}^{13}C][$**SZO$_{300}$**$]$. The $^{13}C\{^1H\}$ CPMAS NMR spectrum of $[Ph_3{}^{13}C][$**SZO$_{300}$**$]$ is shown in Figure 3c. This spectrum contains a signal at 211 ppm, consistent with the formation of a supported trityl cation.[24] Also present in this spectrum are signals for adsorbed $Ph_3{}^{13}CH$ at 57 ppm and adsorbed $Ph_2{}^{13}CH_2$ at 41 ppm. The minor signal at 49 ppm is an unknown impurity. The $^{13}C\{^1H\}$ MAS NMR spectrum of $[Ph_3C][$**SZO$_{300}$**$]$ acquired with sufficiently long recycle delay to obtain quantitative information about the ratio of these peaks is also shown in Figure 3c. From these data, the ratio of $Ph_3{}^{13}C^+ : Ph_3{}^{13}CH : Ph_2{}^{13}CH_2$ is ~4 : 1 : 1. The elemental analysis of $[Ph_3C][$**SZO$_{300}$**$]$ gives 1.16 % C. Using the relative surface coverages from $^{13}C\{^1H\}$ MAS NMR data, there are ~0.04 mmol g^{-1} Ph_3C^+, or ~0.3 Ph_3C^+ nm^{-2}, in this material. This value serves as a rough approximation for pyrosulfate loading in **SZO$_{300}$**, assuming Ph_3CH reacts with all accessible pyrosulfate. Using $Ph_3{}^{13}CH$-d_{15}, where only the phenyl groups are deuterated, gives $[Ph_3C$-$d_{15}][$**SZO$_{300}$**$]$. The ^1H MAS NMR spectrum contains a signal at 4.1 ppm (Figure S22), which is tentatively assigned to the S–H that forms after hydride abstraction by transiently formed SO_3.

The calculated energy of the reaction between Ph_3CH and the pyrosulfate that forms $[Ph_3C][$**SZO$_{300}$**$]$ is −34.7 kcal mol^{-1}. The Ph_3C^+ fragment is planar at the central carbon (Σ_{CCC} = 359.9), as expected for the sp^2 hybridized carbocation. Much like the calculated TEPO*SO_3 and pyridine*SO_3 adducts discussed above, the sulfur has a tetrahedral structure with Σ_{OSO} of 330.8 and S–H bond length of 1.361 Å and S–O bond lengths of 1.454, 1.456, and 1.498, respectively. The calculated S–H stretch is 2501 cm^{-1}, which is close to a weak band at 2590 cm^{-1} in $[Ph_3C][$**SZO$_{300}$**$]$ observed experimentally (Figure S18).

9,10-dihydroanthracene (DHA) reacts with $SbCl_5$ to form isolable $[DHA][SbCl_6]$.[25] DHA-d_4 could serve as a probe for reversible hydride abstraction by transient SO_3 if H/D exchange is observed. Contacting **SZO$_{300}$** with DHA-d_4 (5.4 mmol g^{-1}) at 25 °C in cyclohexane-d_{12} results in a bright orange solid. HD, the expected product that forms from reaction of a Brønsted site with DHA-d_4, was not observed in this reaction (Figure S23). After 60 min at 25 °C the solution phase ^1H NMR spectrum contains signals for DHA-d_0 and DHA-$d_{4\text{-}x}$,[26] indicating that ~79 % of DHA-d_4 undergoes reversible H/D exchange under these conditions. The FTIR of **SZO$_{300}$** after H/D scrambling contains $\nu_{O\text{-}D}$ bands. These bands are not present in **SZO$_{300}$** after soaking in cyclohexane-d_{12} solutions containing DHA, indicating that DHA-d_4 is the source of deuterium. A plausible mechanism for this behavior is shown in Scheme 1. Pyrosulfate sites reversibly abstract deuteride from DHA-d_4 to form the DHA^+. Scrambling of –OD sites with nearby –OH sites and subsequent recombination generates DHA-d_3. Repetition of this sequence results in the observed DHA-d_0 and DHA-$d_{4\text{-}x}$ mixture.

SZO$_{300}$ reacts with iPP or HDPE in the presence of H_2 to form extractable oils, Figure 3a. These reactions were run at low catalyst loadings (0.17 mol %; ~600 monomer units: pyrosulfate), estimated from the pyrosulfate loading in $[Ph_3C][$**SZO$_{300}$**$]$.Over the course of 5 h under 5 atm H_2

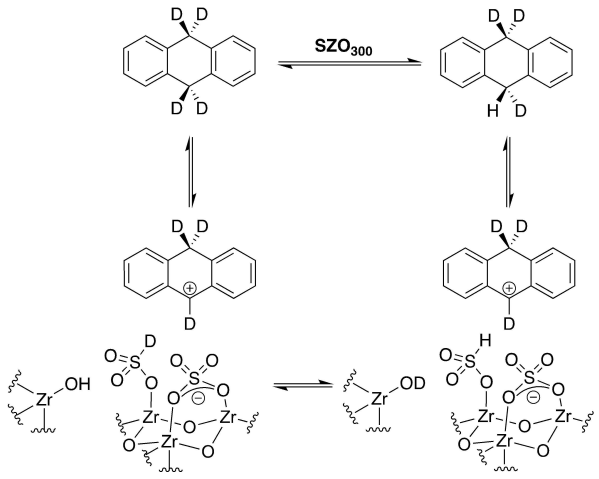

Scheme 1. Proposed reversible H/D exchange mechanism for reactions of **SZO$_{300}$** and DHA-d_4. Repetition of this cycle generates DHA-d_0 and DHA-$d_{4\text{-}x}$.

SZO$_{300}$ reacts with iPP at 200 °C in a neat polymer melt to form an atactic extractable oil soluble in CH_2Cl_2 (M_n = 970 g mol^{-1}, $Đ$ = 3.1) in 51 % yield, Figure 3b. Small amounts of C_1–C_{12} products also form in this reaction. Increasing reaction times beyond 5 h does not increase product yields, suggesting that the catalyst deactivates on this timescale. The spent catalyst is suspended in residual polymer, precluding recycling experiments. Increasing H_2 pressure has a negligible effect on the reaction (Table S2). The M_n values of the oils do not decrease at prolonged reaction times. However, treating the oils with fresh **SZO$_{300}$** does result in reduction of M_n values. In the absence of H_2 extractable oils (M_n = 1100 g mol^{-1}, $Đ$ = 2.9) also form, though in reduced yields. **SZO$_{300}$** also catalyzes hydrogenolysis of commercial iPP food packaging (Figure S54–58), giving oils with similar structures as those obtained with the virgin low MW iPP, though in lower 22 % yield.

We also performed iPP hydrogenolysis with $[tBu_3PH]$-$[$**SZO$_{300}$**$]$.[35] N_2 adsorption of $[tBu_3PH][$**SZO$_{300}$**$]$ (Figure S53) gives a BET surface area of 74 m^2 g^{-1}, the same value as native **SZO$_{300}$**. However, pore volume decreases from 0.19 cm^3 g^{-1} (**SZO$_{300}$**) to 0.063 cm^3 g^{-1} ($[tBu_3PH][$**SZO$_{300}$**$]$) and average BJH pore sizes also decrease from 6.7 nm (**SZO$_{300}$**) to 3.4 nm ($[tBu_3PH][$**SZO$_{300}$**$]$).

$[tBu_3PH][$**SZO$_{300}$**$]$ has significantly lower Brønsted acidity than native **SZO$_{300}$** because acidic –OH groups on this material react with the relatively strong phosphine base ($pK_a(tBu_3PH)$ = 17.0 in MeCN).[27] From phosphine loading (0.12 mmol g^{-1}) and Brønsted loading in **SZO$_{300}$** (0.13 mmol g^{-1}), >90 % of the Brønsted sites react with P^tBu_3. Therefore, reactions mediated or catalyzed by Brønsted sites are expected to be less efficient using $[^tBu_3PH][$**SZO$_{300}$**$]$. Under iPP hydrogenolysis conditions both $[tBu_3PH][$**SZO$_{300}$**$]$ and native **SZO$_{300}$** produce the same yields of extractable oils with essentially identical microstructures (Figure S51–52), indicating that the selectivity of both catalysts is similar. This result suggests that Brønsted acidity has a minimal role in this reaction.

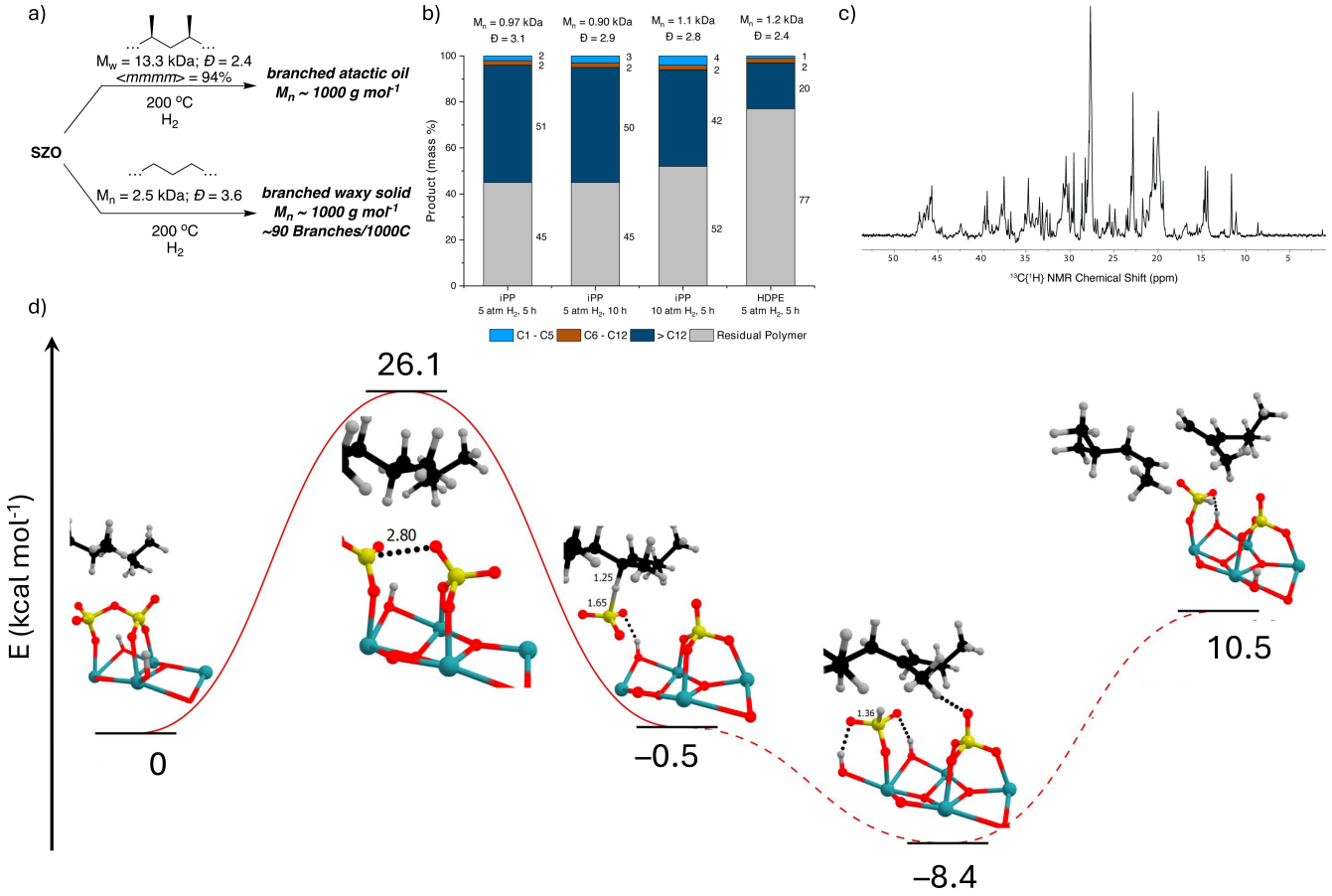

Figure 3. Reaction of **SZO_{300}** with iPP or HDPE to form products (a). Product distribution for polymer degradation reactions (b). A representative quantitative $^{13}C\{^1H\}$ NMR spectra of oils produced with **SZO_{300}** and iPP in the presence of H_2.(c). Calculated potential energy surface for a pyrosulfate reacting with an isotactic propylene tetramer (d).

The microstructure of the oils produced from iPP are complex. A representative quantitative $^{13}C\{^1H\}$ NMR spectra of oils in C_6D_6 at 25 °C are shown in Figure 3c. Virtually indistinguishable $^{13}C\{^1H\}$ NMR spectra are obtained for the other oils described above, though the oils formed in the absence of H_2 contain signals for internal olefins. These spectra contain a dispersion of $–CH_2–$, –CH–, and $–CH_3$ signals consistent with complete loss of diastereoselectivity. These spectra also contain signals between ~30–40 ppm that are assigned to regioirregular errors that appear through chain straightening or related processes under the reaction conditions. Integration of the $–CH_2–$ and regioirregular error signals indicate that the ratio of C_3H_6:regioirregular error is ~1:2, or ~66 % of the main chain in these oils are straightened. Signals for oxygenate functionalities are not present in any of the $^{13}C\{^1H\}$ NMR spectra for any of the oils.

Recovered iPP after hydrogenolysis was also analyzed by NMR spectroscopy at 120 °C in $C_2D_2Cl_4$. The polymer diastereopurity degrades (<*mmmm*> = 71 %), and contains <*mmmr*> (8 %), <*rmmr*> (3 %), <*mmrr*> (7 %), and <*mrrm*> (11 %) errors that are not present in the virgin iPP used in this study. This spectrum also contains signals at 30.60 and 20.74 ppm from chain straightening; ~15 % of the residual iPP is straightened. The $^{13}C\{^1H\}$ NMR spectra of residual iPP also contain minor signals for olefins and carbonyl functionalities (~7 %). **SZO** is known to react with alkanes to form alcohols or ketones via oxygen atom transfer reactions.[28] These side reactions are probably not related to cleavage of iPP chains because oxygenates are not observed in isolated oils, and signals indicating that these oxygenates are at chain ends (i.e. P–C(O)Me) are not present in this spectrum.

HDPE is less reactive than iPP, forming a waxy low molecular weight solid (M_n = 1200 g mol^{-1}, Đ = 2.3) that is freely soluble in hydrocarbon solvents at 25 °C in 21 % yield. NMR analysis of the product indicates that this material contains ~90 branches/1000 C, consistent with a hyperbranched structure that is more typically encountered in ethylene polymerization reactions using late transition metal catalysts.[29]

DFT calculations support the hypothesis that transiently formed SO_3 is responsible for the C–H bond activation step in these reactions. Figure 3d shows the calculated reaction energy diagram for the activation of an isotactic propylene tetramer by the pyrosulfate site on the **SZO** model. The pyrosulfate is maintained when the tetramer is adsorbed onto this model, which is used as a reference point for our

reaction energy diagram. However, the barrier to opening the pyrosulfate to form adsorbed SO_3 and sulfate is only 26.1 kcal mol^{-1}. The first intermediates formed after pyrosulfate opening are best described as alkane adducts of SO_3. Figure 3d shows the reaction profile for reactivity of a tertiary C–H bond, complementary results for a secondary C–H bond are presented in the Supporting Information (Figure S62). The stability of the alkane adduct depends on which C–H bond coordinates to sulfur, if a tertiary C–H coordinates the intermediate is slightly favored (ΔE_{rxn} = −0.5 kcal mol^{-1}). If a secondary C–H bond coordinates to sulfur the intermediate is slightly disfavored (ΔE_{rxn} = 4.8 kcal mol^{-1}). Both intermediates have very similar structure. The d_{CH} is 1.21 Å, significantly longer than a typical sp^3 C–H bond, d_{SH} is 1.81 Å, well within the sum of their van der waal radii, and the S–H–C bond angle is 170°. Abstraction of the C–H bond as a hydride in both cases has a negligible barrier. The tertiary carbocation formed is stable with respect to the tetramer adsorbate (ΔE_{rxn} = −8.3 kcal mol^{-1}), while the secondary carbocation is less stable (ΔE_{rxn} = 13.4 kcal mol^{-1}). The reaction energy significantly increases when a C–H bond in *n*-nonane, a surrogate for the linear HDPE, is activated by the pyrosulfate to form a secondary carbocation (ΔE_{rxn} = 20.9 kcal mol^{-1}, Figure S63).

A plausible reaction that could compete with hydride abstraction is the heterolytic C–H bond activation across a Zr–O sites in this **SZO** model, analogous to that shown in Figure 1c. This reaction is energetically unreasonable using this model. Heterolytic C–H bond activation of a –CH_2– in the tetramer is predicted to have a very high barrier ($\Delta E^{\#}$ = 55.2 kcal mol^{-1}) to form an unstable Zr–R species (ΔE_{rxn} = 36.8 kcal mol^{-1}) on this flat ZrO_2 model. These values are significantly higher than those obtained in C–H bond activation reactions with amorphous ZrO_2 models where this mechanism has more favorable energetics.[7]

Once the carbocation is formed β-scission cleaves the polymer chain to give an olefin and a secondary carbocation.[30] In the presence of H_2, hydrogenation of the olefin forms alkanes. ZrO_2 materials are known to heterolytically activate H_2 to form Zr–H sites,[31] and to catalyze olefin hydrogenation reactions.[32] Reactions performed in the presence of D_2 incorporate deuterium in the –CH_2– and –CH_3 positions of the oils (Figure S53), suggesting the sequence of reactions shown in Scheme 2. After chain cleavage from the 3° carbocation, the secondary carbocation transfers a proton to the vinylidene fragment to form a terminal olefin and a new 3° carbocation. Addition of D_2 to the terminal olefin gives the observed selectivity. Isomerization of the terminal olefin in the absence of H_2 forms the internal olefins that are observed under those conditions.

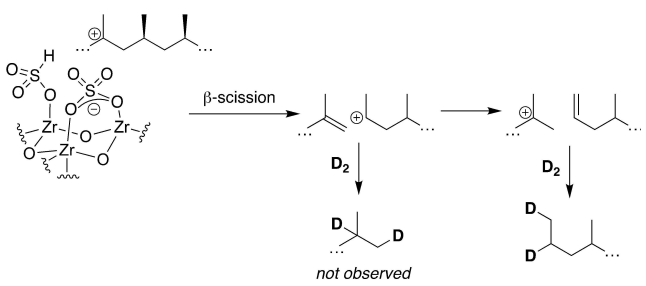

Scheme 2. D_2 labelling shows incorporation of deuterium into –CH_2– and –CH_3 positions.

Sulfated zirconium oxide (**SZO**) is an enigmatic material with a rich and complex history. Selected properties are described in Figure 4. Initial reports showed that **SZO** forms isobutane from butane at lower temperatures than oleum, which was attributed to Brønsted "superacid" sites on this material.[33] Implicit in this proposal is that carbocations form by protonation of butane to form carbocations, analogous to liquid superacids.[34] However, DFT studies of fully dehydrated ZrO_2 showed that H_2SO_4 heterolytically dissociates to form Zr–(OH)–Zr Brønsted sites near bound sulfate anions, which are mild Brønsted acids from gas phase acidity calculations.[22] This is supported by experimental studies showing that **SZO** does not protonate *p*-nitroaniline in MeCN slurry (pK_a(anilinium) = 6.22 in MeCN).[35] Though mild, the Brønsted sites on **SZO** participate in reactions with organometallics to form well-defined ion-pairs where the sulfate behaves as a weakly coordinating anion.[10]

SZO also shows pronounced redox activity. Lercher and Sauer showed that butane adsorbs onto **SZO** to form butenes, and careful measurement of byproducts formed during butane isomerization detected SO_2 as a byproduct.[13] DFT calculations also showed that the overall reaction of pyrosulfates and butane to form sulfate, SO_2, H_2O and butene is exothermic. The butene generated in this reaction was proposed to react with the mild Brønsted sites on **SZO** to form the supported carbocation ion (or alkoxide) that rearranges to isobutane. This result also explains why butene promotes the butane isomerization reaction.[36] A mechanistically related reaction was reported by Delferro and Kaphan in reactions of Cp*IrPh(Me)(PMe_3) with pyrosulfate sites on sulfated alumina.[14] In this case, single electron transfer from Cp*IrPh(Me)(PMe_3) to a pyrosulfate forms a [$SO_3^{\bullet}$][SO_4^-] site that abstracts an H-atom from the Cp* ligand.[14] The latter example is the closest to the pyrosulfate opening to transient SO_3 and SO_4^{2-} sites proposed here.

The formation of carbocations on **SZO** is generally inferred to be a result of a "superacidic" Brønsted site. Because **SZO** is a mild Brønsted acid, reactions with alkanes through traditional mechanisms encountered with liquid[34] or solid[37] superacids are not possible. A Brønsted acidity argument also neglects plausible reaction pathways that could be mediated by strong Lewis acids present in superacids.[38] In this case, the pyrosulfate site serves as a reservoir of adsorbed SO_3 on the **SZO** surface that facilitates reversible hydride abstraction of sp^3 hybridized C–H bonds to form carbocations that can undergo subsequent reaction chemistry (Figure 4, red structures).

Pyridine and TEPO are common acidity probes. Both probes form strong adducts that are (essentially) irreversible on surfaces, and both provide a spectroscopic readout for the quantity and strength of acid sites. Related calorimetry studies were described by Drago and Kob using pyridine to determine acid strength of sites present on **SZO**.[39] Those

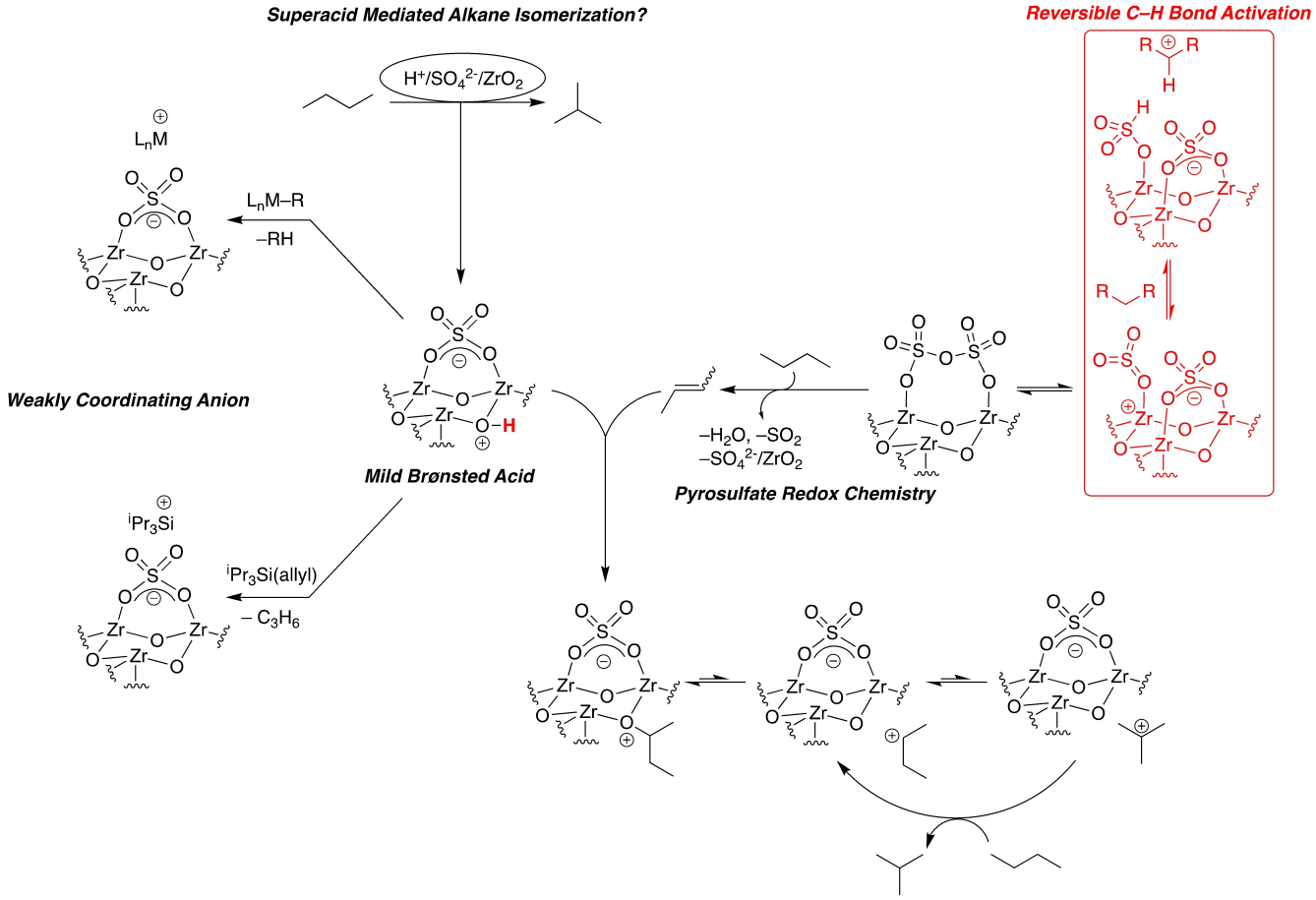

Figure 4. Selected key properties of sulfated zirconium oxide (**SZO_{300}**).

studies found that pyridine binds to a strong acid site with an energy of 31.2 kcal mol^{-1}, close to the value calculated for adduct formation between the pyrosulfate and pyridine described here.

However, the calculated adduct formation energy between pyridine and pyrosulfate of −39.7 kcal mol^{-1}, while significantly more exothermic than pyridine binding to a Zr-Lewis site (−32.3 kcal mol^{-1}), is weaker than expected for a strong Lewis acid. For example, the very strong tricoordinate aluminum Lewis site on Al_2O_3, which activates C–H bonds by a heterolytic mechanism,[40] forms an adduct with pyridine that has a calculated adduct formation energy of up to −50 kcal mol^{-1}.[41]

Two explanations can account for this discrepancy. First, adduct formation between pyridine and pyrosulfate should not be viewed as classical adsorption onto a "bare" Lewis site on an oxide. The calculated adduct formation energy is a composite the strong N→S interaction (exothermic) and the breaking of the S–O bond in the pyrosulfate (endothermic). This reduces the overall adduct formation energy compared to the more standard adsorption energy onto a bare Lewis site because bonds are generally not broken in the latter case. Second, sterics probably reduces the overall binding energy in py*SZO compared to the more sterically accessible oxygen in TEPO or the C–H bond in Ph_3CH. This is reflected in the sum of the O–S–O bond angles (Σ_{OSO}). In py*SZO the Σ_{OSO} is 348.4°, which is far larger than Σ_{OSO} for TEPO*SO_3 (332.85°) or Ph_3CH*SO_3 (330.8°).

DFT calculations show that the reaction between the pyrosulfate and alkanes to form carbocations is Ph_3CH >3° C–H >2° C–H, which is expected based on the stabilities of these carbocations after hydride abstraction. The calculated energies also relate to the hydride ion affinity of the adsorbed SO_3 site. Using the calculated gas-phase heterolytic C–H bond strengths for Ph_3CH (191.5 kcal mol^{-1})[42] or the experimental value for the 2° C–H in C_3H_6 (251.6 kcal mol^{-1})[43] brackets the hydride ion affinity of adsorbed SO_3 between 226.2 to 237.9 kcal mol^{-1}. This value is larger than the calculated hydride ion affinity of Me_3Si^+ (220.8 kcal mol^{-1}) or SbF_5 (127.4 kcal mol^{-1}),[44] the latter of which is generally accepted as the threshold for a Lewis superacid. From this analysis the SO_3 site is, to our knowledge, the strongest formally neutral Lewis acid reported in the literature.

After the carbocation is formed polymer chains can be cleaved by β-scission reactions. The data in Figure 3b show that iPP is more reactive to chain-scission than HDPE. This is not surprising. Pyrolysis of these polymers in the absence of catalyst shows that HDPE reacts ~130 °C higher than iPP.[45] This trend extends to well-defined Ta–H species that

catalyze hydrogenolysis of iPP with greater efficiency than HDPE under identical conditions.[46] The origins of this behavior could be related to the steric environment of the reactive intermediates formed under these conditions, which are known to influence β-scission reactions.[30,47] In this case, formation of a relatively stable 3° carbocation after C–H bond activation facilitates chain-scission relative to formation of an unstable 2° carbocation.

Formation of a carbocation also allows isomerization reactions to occur. This is evident in the polymer hydrogenolysis chemistry described in Figure 3. Both iPP and HDPE react under these conditions to form extractable oils containing quite complex microstructures. Classic carbocation chemistry can explain these observations. The complete loss of tacticity in oils formed during iPP hydrogenolysis can be explained by fast 1,3-hydride shifts, a process known to occur with a barrier of 8.5 kcal mol^{-1} in the 2,4-dimethyl-2-pentyl cation, eq 1.[48] The hyperbranched structure obtained from HDPE hydrogenolysis results from formation of a secondary carbocation followed by 1,2-migration that forms a tertiary carbocation and a branch, eq 2. 1,2-migrations also form regioirregular errors in iPP oils and is responsible for chain-straightening in residual iPP.

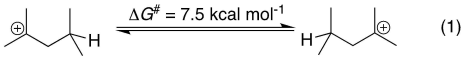

(1)

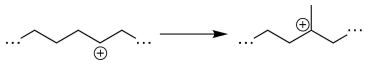
(2)

Conclusion

Sulfated zirconium oxide (**SZO**) does not activate C–H bonds by the traditional σ-bond metathesis or heterolytic cleavage mechanisms that are commonly encountered on oxide surfaces. Brønsted sites on **SZO**, commonly invoked as reactive species in reactions with alkanes, are also not responsible for C–H bond activation. Instead, reactive pyrosulfate sites open to form adsorbed SO_3 and sulfate. Transiently adsorbed SO_3 is a very strong Lewis acid that polarizes C–H bonds and abstracts hydrides to form carbocations. Both experimental data and computational modeling shows that this reaction is reversible. However, Brønsted or Zr-Lewis sites proximal to the pyrosulfate could affect this reactivity significantly. More studies are needed to determine these effects.

The surface chemistry of **SZO** is distinctly complex, yet this material is prepared from very simple precursors and derivatives are used industrially in alkane isomerization reactions.[49] This is potentially attractive in the context of polymer upcycling reactions that generally feature noble metal nanoparticles or air/moisture sensitive organometallics as active catalysts for these reactions. Clear limitations persist, however. Not addressed in this contribution is the deactivation of the pyrosulfate site, which likely proceeds by reduction of SO_3 to SO_2 and water.[13] Increasing productivity of **SZO** in polymer degradation is required. Two plausible strategies are oxidation of SO_2 back to SO_3, which will likely also introduce competitive polymer oxidation reactions that could outcompete catalysis, or modifications of the oxide to prevent or restrict reduction of SO_3 to SO_2.

Acknowledgements

This research was supported by Chevron Phillips Chemical LP. Solid-state NMR measurements were supported by the U.S. Department of Energy, Office of Basic Energy Sciences, Catalysis Science program (DE-SC0022203). The use of supercomputer facilities was sponsored by NWO Domain Science. AAK and EAP thank to Dr. Maicon Delarmenia (Cardiff University) for providing the sulfated zirconia models, which greatly facilitated our calculations. MPC thanks Prof. William J. Neary for providing access to the room temperature GPC used in this study.

Conflict of Interest

A patent application has been filed PCT/US2023/072971.

Data Availability Statement

The data that support the findings of this study are available from the corresponding author upon reasonable request.

Keywords: C–H Bond Activation · Lewis Acid · Carbocation · Heterogeneous Catalysis · Solid-state NMR

[1] a) P. F. Britt, G. W. Coates, K. I. Winey, J. Byers, E. Chen, B. Coughlin, C. Ellison, J. Garcia, A. Goldman, J. Guzman, J. Hartwig, B. Helms, G. Huber, C. Jenks, J. Martin, M. McCann, S. Miller, H. O'Neill, A. Sadow, S. Scott, L. Sita, D. Vlachos, R. Waymouth, *Report of the Basic Energy Sciences Roundtable on Chemical Upcycling of Polymers*, United States, **2019**; b) J. Sun, J. Dong, L. Gao, Y.-Q. Zhao, H. Moon, S. L. Scott, *Chem. Rev.* **2024**, *124*, 9457–9579.
[2] J. Hartwig, *Organotransition Metal Chemistry*, University Science Books, **2010**.
[3] a) J. D. A. Pelletier, J.-M. Basset, *Acc. Chem. Res.* **2016**, *49*, 664–677; b) F. Rataboul, A. Baudouin, C. Thieuleux, L. Veyre, C. Copéret, J. Thivolle-Cazat, J.-M. Basset, A. Lesage, L. Emsley, *J. Am. Chem. Soc.* **2004**, *126*, 12541–12550.
[4] R. Waterman, *Organometallics* **2013**, *32*, 7249–7263.
[5] C. Coperet, *Chem. Rev.* **2010**, *110*, 656–680.
[6] P. T. Wolczanski, *Organometallics* **2018**, *37*, 505–516.
[7] S. Chen, A. Tennakoon, K.-E. You, A. L. Paterson, R. Yappert, S. Alayoglu, L. Fang, X. Wu, T. Y. Zhao, M. P. Lapak, M. Saravanan, R. A. Hackler, Y.-Y. Wang, L. Qi, M. Delferro, T. Li, B. Lee, B. Peters, K. R. Poeppelmeier, S. C. Ammal, C. R. Bowers, F. A. Perras, A. Heyden, A. D. Sadow, W. Huang, *Nature Catalysis* **2023**, *6*, 161–173.
[8] a) Zeolites also activate C–H bonds to form carbocations, see: C. Chizallet, C. Bouchy, K. Larmier, G. Pirngruber, *Chem. Rev.* **2023**, *123*, 6107–6196; b) A. Corma, H. García, *Chem. Rev.* **2002**, *102*, 3837–3892; c) A. Feller, J. A. Lercher, in *Adv. Catal., Vol. 48*, Academic Press, **2004**, pp. 229–295.

[9] G. X. Yan, A. Wang, I. E. Wachs, J. Baltrusaitis, *Appl. Catal. A* **2019**, *572*, 210–225.
[10] a) R. J. Witzke, A. Chapovetsky, M. P. Conley, D. M. Kaphan, M. Delferro, *ACS Catal.* **2020**, 11822–11840; b) K. K. Samudrala, M. P. Conley, *Chem. Commun.* **2023**, *59*, 4115–4127; c) M. Stalzer, M. Delferro, T. Marks, *Catal. Lett.* **2015**, *145*, 3–14.
[11] S. R. Cleary, A. K. Starace, C. C. Curran-Velasco, D. A. Ruddy, C. M. McGuirk, *Langmuir* **2024**, *40*, 6612–6653.
[12] a) A. D. Sadow, T. D. Tilley, *Organometallics* **2003**, *22*, 3577–3585; b) J. Gao, L. Zhu, M. P. Conley, *J. Am. Chem. Soc.* **2023**, *145*, 4964–4968; cQ. Lai, A. H. Mason, A. Agarwal, W. C. Edenfield, X. Zhang, T. Kobayashi, Y. Kratish, T. J. Marks, *Angew. Chem. Int. Ed.* **2023**, *62*, e202312546.
[13] X. Li, K. Nagaoka, L. J. Simon, R. Olindo, J. A. Lercher, A. Hofmann, J. Sauer, *J. Am. Chem. Soc.* **2005**, *127*, 16159–16166.
[14] R. C. Klet, D. M. Kaphan, C. Liu, C. Yang, A. J. Kropf, F. A. Perras, M. Pruski, A. S. Hock, M. Delferro, *J. Am. Chem. Soc.* **2018**, *140*, 6308–6316.
[15] a) M. Bensitel, O. Saur, J. C. Lavalley, B. A. Morrow, *Mater. Chem. Phys.* **1988**, *19*, 147–156; bC. Morterra, G. Cerrato, V. Bolis, *Catal. Today* **1993**, *17*, 505–515; cD. J. Rosenberg, B. Bachiller-Baeza, T. J. Dines, J. A. Anderson, *J. Phys. Chem. B* **2003**, *107*, 6526–6534.
[16] W.-H. Chen, H.-H. Ko, A. Sakthivel, S.-J. Huang, S.-H. Liu, A.-Y. Lo, T.-C. Tsai, S.-B. Liu, *Catal. Today* **2006**, *116*, 111–120.
[17] J. F. Haw, J. Zhang, K. Shimizu, T. N. Venkatraman, D.-P. Luigi, W. Song, D. H. Barich, J. B. Nicholas, *J. Am. Chem. Soc.* **2000**, *122*, 12561–12570.
[18] A. Zheng, S.-B. Liu, F. Deng, *Chem. Rev.* **2017**, *117*, 12475–12531.
[19] H. Großekappenberg, M. Reißmann, M. Schmidtmann, T. Müller, *Organometallics* **2015**, *34*, 4952–4958.
[20] H. F. T. Klare, L. Albers, L. Süsse, S. Keess, T. Müller, M. Oestreich, *Chem. Rev.* **2021**, *121*, 5889–5985.
[21] D. B. Culver, M. P. Conley, *Angew. Chem. Int. Ed.* **2018**, *57*, 14902–14905.
[22] F. Haase, J. Sauer, *J. Am. Chem. Soc.* **1998**, *120*, 13503–13512.
[23] S. Brownstein, E. Gabe, F. Lee, B. Louie, *J. Org. Chem.* **1988**, *53*, 951–954.
[24] Formation of trityl cations on zeolites by chloride abstraction from Ph_3CCl, see: a) T. Tao, G. E. Maciel, *Langmuir* **1999**, *15*, 1236–1246; b) $Ph_3{}^{13}C^+$ also forms on a SZO with significantly lower sulfate loading (~3 S-containing anions per nm^2), suggesting that pyrosulfate forms on sulfated zirconia with significantly lower sulfate loading.
[25] J. Holmes, R. Pettit, *J. Org. Chem.* **1963**, *28*, 1695–1696.
[26] At room temperature this mixture slowly converts to anthracene and tetrahydroanthracene. Deuterium does not incorporate into these products to an appreciable extent. We are currently studying this reaction in more detail, and will report the results separately.
[27] K. Abdur-Rashid, T. P. Fong, B. Greaves, D. G. Gusev, J. G. Hinman, S. E. Landau, A. J. Lough, R. H. Morris, *J. Am. Chem. Soc.* **2000**, *122*, 9155–9171.
[28] D. Farcasiu, A. Ghenciu, J. Q. Li, *J. Catal.* **1996**, *158*, 116–127.
[29] a) L. Guo, S. Dai, X. Sui, C. Chen, *ACS Catal.* **2016**, *6*, 428–441; b) C. Tan, C. Chen, *Angew. Chem. Int. Ed.* **2019**, *58*, 7192–7200; c) S. D. Ittel, L. K. Johnson, M. Brookhart, *Chem. Rev.* **2000**, *100*, 1169–1204.
[30] a) M. N. Mazar, S. Al-Hashimi, M. Cococcioni, A. Bhan, *J. Phys. Chem. C* **2013**, *117*, 23609–23620; b) J. Rey, C. Bignaud, P. Raybaud, T. Bučko, C. Chizallet, *Angew. Chem. Int. Ed.* **2020**, *59*, 18938–18942.
[31] T. Onishi, H. Abe, K.-i. Maruya, K. Domen, *Chem. Commun.* **1985**, 617–618.
[32] J. Kondo, K. Domen, K.-i. Maruya, T. Onishi, *J. Chem. Soc. Faraday Trans.* **1992**, *88*, 2095–2099.
[33] M. Hino, S. Kobayashi, K. Arata, *J. Am. Chem. Soc.* **1979**, *101*, 6439–6441.
[34] G. A. Olah, G. K. S. Prakash, J. Sommer, A. Molnar, *Superacid Chemistry*, John Wiley & sons, **2009**.
[35] J. Rodriguez, D. B. Culver, M. P. Conley, *J. Am. Chem. Soc.* **2019**, *141*, 1484–1488.
[36] J. E. Tabora, R. J. Davis, *J. Am. Chem. Soc.* **1996**, *118*, 12240–12241.
[37] C. A. Reed, *Acc. Chem. Res.* **2013**, *46*, 2567–2575.
[38] a) C. R. King, A. Holdaway, G. Durrant, J. Wheeler, L. Suaava, M. M. Konnick, R. A. Periana, D. H. Ess, *Dalton Trans.* **2019**, *48*, 17029–17036; b) S.-S. Chen, A. Koppaka, R. A. Periana, D. H. Ess, *J. Am. Chem. Soc.* **2021**, *143*, 18242–18250.
[39] R. S. Drago, N. Kob, *J. Phys. Chem. B* **1997**, *101*, 3360–3364.
[40] a) R. Wischert, P. Laurent, C. Copéret, F. Delbecq, P. Sautet, *J. Am. Chem. Soc.* **2012**, *134*, 14430–14449; b) R. Wischert, C. Copéret, F. Delbecq, P. Sautet, *Angew. Chem. Int. Ed.* **2011**, *50*, 3202–3205.
[41] I. B. Moroz, K. Larmier, W.-C. Liao, C. Copéret, *J. Phys. Chem. C* **2018**, *122*, 10871–10882.
[42] S. A. Couchman, D. J. D. Wilson, J. L. Dutton, *Eur. J. Org. Chem.* **2014**, *2014*, 3902–3908.
[43] S. K. Shin, J. L. Beauchamp, *J. Am. Chem. Soc.* **1989**, *111*, 900–906.
[44] P. Erdmann, L. Greb, *ChemPhysChem* **2021**, *22*, 935–943.
[45] I. Vollmer, M. J. F. Jenks, M. C. P. Roelands, R. J. White, T. van Harmelen, P. de Wild, G. P. van der Laan, F. Meirer, J. T. F. Keurentjes, B. M. Weckhuysen, *Angew. Chem. Int. Ed.* **2020**, *59*, 15402–15423.
[46] J. Gao, L. Zhu, M. P. Conley, *ACS Catal.* **2023**, 10765–10769.
[47] M. E. O'Reilly, S. Dutta, A. S. Veige, *Chem. Rev.* **2016**, *116*, 8105–8145.
[48] M. Saunders, J. J. Stofko, *J. Am. Chem. Soc.* **1973**, *95*, 252–253.
[49] T. Kimura, *Catal. Today* **2003**, *81*, 57–63.

Manuscript received: November 7, 2024
Accepted manuscript online: December 23, 2024
Version of record online: January 10, 2025